Semi-Transparent p-Cu O/n-ZnO Nanoscale-Film Heterojunctions for Photodetection and Photovoltaic Applications

Claudia de Melo, Maud Jullien, Yann Battie, Aotmane En Naciri, Jaafar Ghanbaja, François Montaigne, Jean-François Pierson, Federica Rigoni, Nils Almqvist, Alberto Vomiero, et al.

Semi-Transparent p-Cu_2O/n-ZnO Nanoscale-Film Heterojunctions for Photodetection and Photovoltaic Applications

Claudia de Melo[†‡], Maud Jullien[†], Yann Battie[§], Aotmane En Naciri[§], Jaafar Ghanbaja[†], François Montaigne[†], Jean-François Pierson[†], Federica Rigoni[‖], Nils Almqvist[‖], Alberto Vomiero[‖], Sylvie Migot[‡], Frank Mücklich[‡], David Horwat[†]*

[†] Université de Lorraine, CNRS, IJL, F-54000 Nancy, France

[‡] Department of Materials Science and Engineering, Saarland University, D-66123 Saarbrücken, Germany

[§] LCP-A2MC, Institut Jean Barriol, Université de Lorraine, 1 Bd Arago, 57070 Metz, France

[‖] Department of Engineering Sciences and Mathematics, Division of Materials Science, Luleå University of Technology, 971 87 Luleå, Sweden

KEYWORDS: copper oxide, atomic layer deposition, local epitaxy, heterojunction, transparent electronics, photodetectors.

ABSTRACT: Transparent nanoscale-film heterojunctions based on Cu_2O and ZnO were fabricated by atomic layer deposition and reactive magnetron sputtering. The constitutive layers exhibit high crystalline quality and a local epitaxial relation between Cu_2O and ZnO was achieved with [110] Cu_2O || [001] ZnO and [001] Cu_2O || [010] ZnO as evidenced by high resolution transmission

electron microscopy and. Cu_2O films show very low resistivity and high mobility values of 9 - 150 Ω cm and 19 cm^2 / V s, respectively. The Cu_2O/ZnO heterojunctions exhibit a non-linear rectifying behavior characteristic of a p-n junction, self-powered photo-response under 1-Sun illumination and an average transmittance of 73% in the visible region of the electromagnetic spectrum. These results are promising for all-oxide transparent electronics, photodetection and photovoltaic applications.

Introduction

Metal oxide semiconductors have gained a lot of attention owing to their good chemical stability, abundance of constitutive elements in the earth crust, non-toxicity and low-fabrication cost. They can find application in a wide variety of fields like optoelectronics,[1] photovoltaics,[2,3] water splitting,[4] and photodetection,[5,6] among others.[7,8] Furthermore, the fabrication of all-oxide based devices is emerging as an approach to reduce manufacturing cost and environmental impact. Cu_2O/ZnO heterojunctions can become important building elements of such devices.

ZnO is a n-type transparent conductive oxide (TCO) with a wide band gap of 3.37 eV, large exciton binding energy of 60 meV, high electron mobility, and high thermal conductivity. These properties make it an ideal candidate for UV photodetection, light emitting diodes, transparent thin film transistors, transparent contacts and window layer in solar cells.[9] Since most of the TCOs are n-type materials and achieving p-type doping of these material is challenging, the creation of an homojunction is a difficult task. Therefore, the research has focused on finding appropriate partner layers to form heterojunction devices based on oxides. Cu_2O is among the most promising p-type semiconductor oxides, with a bandgap of 2.1-2.5 eV and high hole mobility (~100 $cm^2V^{-1}s^{-1}$ in single crystal Cu_2O). Moreover, its large absorption coefficient makes it suitable for photovoltaic applications: as p-type absorber layer in combination with n-type wide bandgap semiconductor

oxides such as ZnO, TiO_2, and Ga_2O_3 [10–12], as hole transport layer in perovskite solar cells,[13] and as top cell of Si-based tandem solar cells in combination with ZnO.[14] With its relatively large bandgap Cu_2O is considered as suitable for thin film transparent and semi-transparent photovoltaics applications in combination with ZnO.[15] Cu_2O/ZnO heterojunctions have been also investigated for visible and UV photodetection.[16,17] In particular, self-powered photodetectors have gained a lot of attention in recent years due to their autonomous and sustainable operation without the need of an external bias. This make it suitable building blocks of optoelectronic devices, portable electronics, environmental monitoring and for future "smart" sensors networks. [18–20] Several studies have been dedicated to the fabrication of ZnO-based p–n self-powered photodetectors operating between the UV and visible regions of the spectra.[20–22] Recent developments include the possibility of tuning the photocurrent polarity in a ZnO nanowires/SnS photodetector with the wavelength of the incoming light.[19] Cu_2O/ZnO nanostructures devices have also shown promises in this field. Fast response photodetectors have been obtained in a ZnO/Cu_2O core-shell nanowires architecture[5], and high photoresponse and fast response times were also reported for a Cu_2O/ZnO-nanorods heterojunction at 0 bias voltage, under UV and blue-light excitation.[23] Enhanced photoresponse and faster response times were also reported by Bai *et al.* in a ZnO/Cu_2O/electrolyte heterojunctions by the incorporation of graphene interlayers.[24]

In this work we report on the fabrication and response of semi-transparent Cu_2O/ZnO nanoscale-heterojunctions, consisting on a simpler bi-layer architecture, compared with the typical nanostructured devices mentioned previously. The fabrication of the Cu_2O thin films by atomic layer deposition results in high quality thin films and very smooth interface with ZnO thanks to local domain epitaxial matching between both oxides. The possibility of fabricating nanoscale-transparent heterojunctions based on these materials is demonstrated, which is highly sought for

transparent photovoltaics and all-oxide transparent electronics. Furthermore, the presence of a self-powered stable photoresponse under 1 Sun irradiation is of strong interest for visible photodetection applications.

Experimental

ZnO films were deposited on (100) Si, glass and ITO/glass substrates by reactive magnetron sputtering of Zn target with 99.995 % purity (HMW Hauner GmbH & Co. KG). The substrates were placed on a rotating substrate holder next to the magnetron axis and the distance between the target and the substrates was 5 cm (see schematic in Figure 1). An Advanced Energy MDX 1.5 kW DC power supply was used to sputter the Zn target. The current applied to the target was fixed at 0.07 A. Ar and O_2 flow rates of 50 sccm and 8 sccm were employed, respectively. The samples were deposited at a total pressure of 0.5 Pa and no intentional heating was employed during the growth. Under these conditions, a growth rate of 5.3 nm/min was obtained.

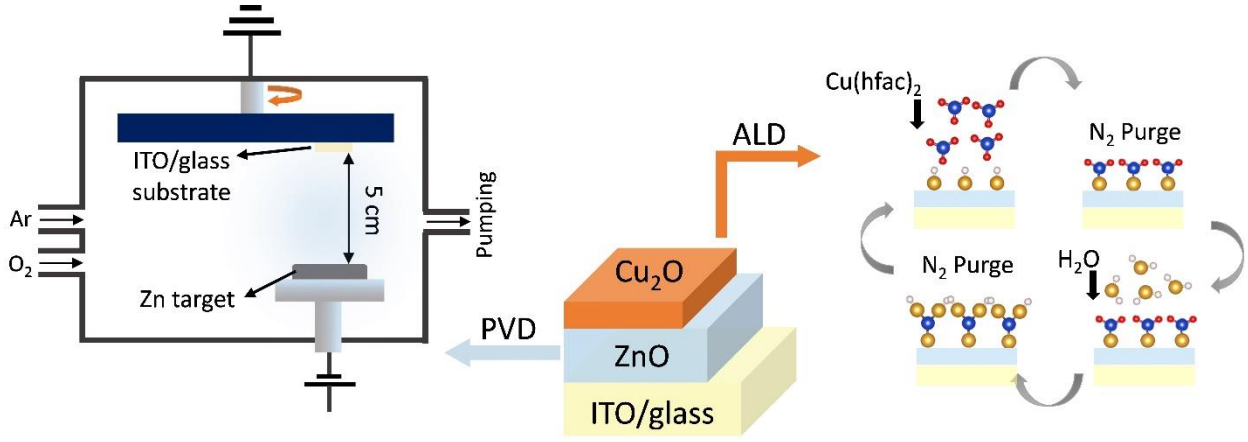

Figure 1. Schematic of the fabrication methods for the Cu_2O/ZnO heterojunction on ITO/glass substrates.

In previous studies we have reported on the area-selective ALD growth of Cu_2O and metallic Cu thin films on ZnO substrates using the $Cu(hfac)_2$ precursor, in the temperature window 240 - 300°C.[25,26] In the present work we use the optimized conditions for the growth of single phase

Cu_2O. Cu_2O films were grown on top of the ZnO thin films by atomic layer deposition in an ALD PICOSUN™ R-200 Advanced reactor. Copper (II) hexafluoro acetyl acetonate, known as $Cu(hfac)_2$, was used as copper precursor (99.99+%-Cu, Stream Chemicals) and was delivered to the reactor by N_2 carrier gas flowing at 150 sccm. Deionized water was used as reactant and was introduced into the reactor through a different line using N_2 carrier gas at a flow rate of 120 sccm. One ALD cycles consisted in a $Cu(hfac)_2$ pulse of 1 s, a first N_2 purge of 6 s, followed by a 3 s pulse of H_2O and 6 s of N_2 purge. The $Cu(hfac)_2$ was sublimated at 70°C and the water bottle was kept at room temperature. The temperature of the reaction chamber was 280°C and the number of cycles was 10 000, which resulted in a growth per cycle (GPC) of 0.04 Å/cycle.

X-ray diffraction analysis was performed to the samples in a Bruker D8 Advanced diffractometer with Cu $K_{\alpha 1}$ radiation using the Bragg-Brentano configuration. Electrical measurements were performed to the Cu_2O films by the four-point probe method and by a Hall measurement system (Ecopia, HMS-5000) in the van der Pauw geometry. Transmittance and reflectance measurements were performed to the ZnO (250 nm) and Cu_2O (40 nm) films deposited on glass and sapphire substrates, respectively, by a Cary UV–Vis–NIR 5000 spectrophotometer. Ellipsometric measurements were carried out using a phase-modulated ellipsometer (UVISEL, Horiba Jobin Yvon) in the spectral range 0.6 eV - 4.6 eV at two angles of incidence, 60° and 70°. Top-view micrographs were performed by scanning electron microscopy (SEM) in a Philips XL-30 S-FEG SEM at 5 kV. Transmission electron microscopy (TEM) was performed to the samples by a JEOL ARM 200-Cold FEG (point resolution 0.19 nm). For this analysis, cross-section TEM samples were prepared using a focused ion beam (FIB) FEI Helios 600. Composition profiles were obtained by energy dispersive spectroscopy (EDS) in scanning transmission electron microscopy (STEM) mode. The electrical characterization of the Cu_2O/ZnO heterojunction was conducted using a

source picometer (Keithley 2401). For the measurement under 1 Sun illumination, a solar simulator was employed, consisting in a xenon arc lamp with an AM 1.5G filter (1000 W/m^2).

Results and discussion

Figure 2a shows the X-ray diffractogram of a typical Cu_2O/ZnO/Si sample. The ZnO films are c-axis oriented as only the 00l diffraction lines of wurtzite crystal structure of ZnO are observed. Cu_2O films are textured with the [110] direction parallel to the ZnO c-axis, since only the hh0 diffraction lines are observed. The morphology of the ZnO and Cu_2O films can be seen at the top-view SEM micrograph (Figure 2b, c).

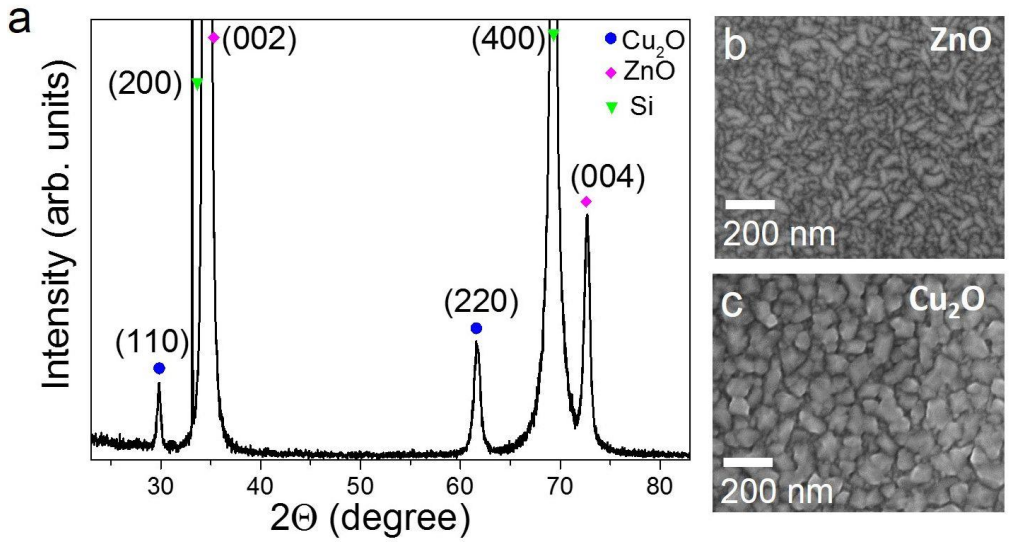

Figure 2. (a) X-ray diffractogram of the Cu_2O/ZnO heterojunction on a Si substrate. (b) Top-view SEM micrograph of the ZnO (b) and Cu_2O (c) films.

Figure 3a shows a cross-section TEM micrograph of a ZnO film on Si. An amorphous SiO_2 native oxide layer of around 5 nm is observed at the interface between the Si substrate and the ZnO film. The film presents a c-axis oriented columnar microstructure in agreement with the X-ray diffractograms. A high-resolution TEM (HR-TEM) micrograph taken to the region enclosed by a white square is shown in Figure 3b with the corresponding fast Fourier transform pattern. The

lattice spacing of the (002) crystallographic planes is 2.609 Å in good agreement with the values reported for hexagonal wurtzite ZnO (PDF 00-036-1451). A HR-TEM micrograph of Cu_2O film grown on ZnO/Si is shown in Figure 3c. In Figure 3d, the lattice spacing of the (110) and (220) planes are indicated with values of 3.017 Å and 1.509 Å, respectively, in agreement with the values reported for cubic Cu_2O (JCPDS 04-007-9767).

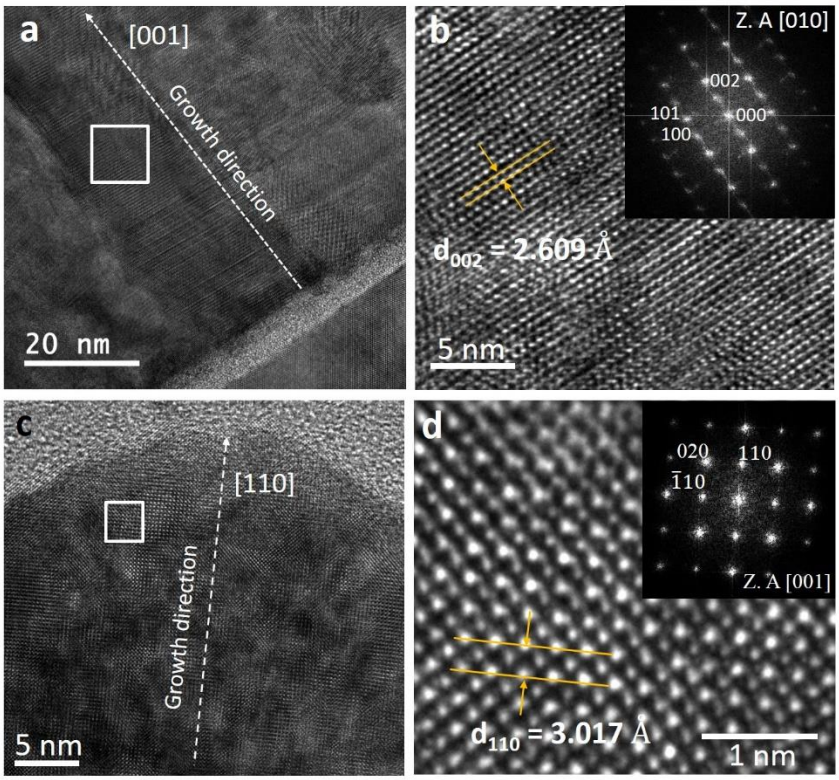

Figure 3. (a) Cross-section TEM micrograph of the ZnO film. (b) HR-TEM micrograph at the region highlighted by a white square, the (002) planes are indicated and the FFT pattern is shown as inset. (c) HR-TEM micrograph of the Cu_2O film. (d) Magnified HR-TEM micrograph of the Cu_2O film showing the (110) planes, the corresponding FFT pattern is shown as inset.

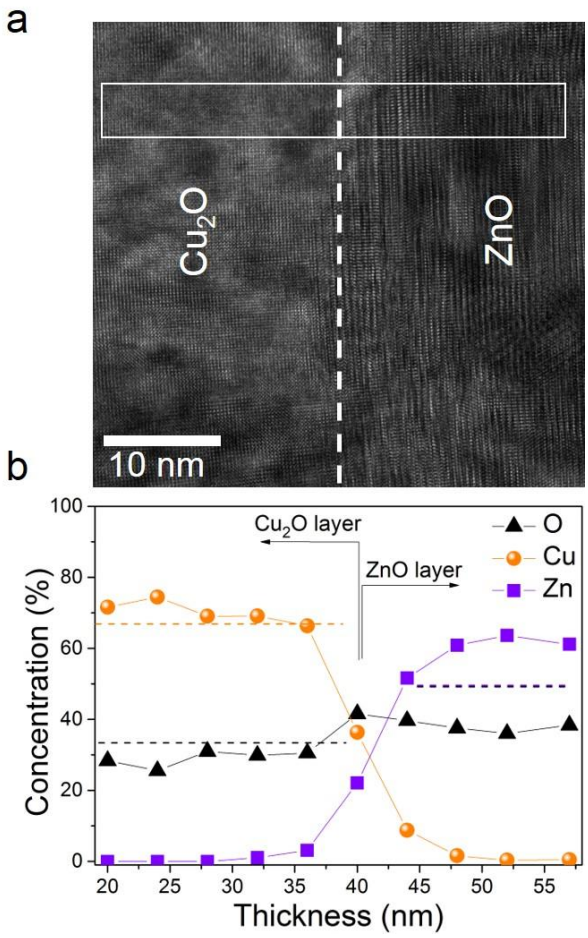

Figure 4. (a) High-resolution TEM micrograph of the heterojunction interface. (b) Composition profiles obtained by EDS in the region enclosed by a rectangle in a (dashed lines indicate the expected Cu, Zn and O concentrations for the stoichiometric Cu_2O and ZnO).

A bright field STEM micrograph taken at the interface between Cu_2O and ZnO is presented in Figure 4 a. EDS analysis was performed in the region enclosed by a white rectangle. The compositional profiles for Cu (orange), Zn (violet) and O (black) are displayed in Figure 4b (dashed lines indicate the expected concentration for stoichiometric Cu_2O and ZnO). The ZnO film presents sub-stoichiometry in oxygen, however, this does not affect the film properties to a great extent since transparency is still very high, as will be shown later. On the other hand, for the Cu_2O

film the atomic concentration obtained for copper (~ 69 %) and oxygen (~ 31 %) are in relatively good agreement with those expected for the stoichiometric material.

Local epitaxial relationship and domain epitaxial matching

The texture of the Cu_2O film on ZnO with (110) Cu_2O || (001) ZnO, observed in the X-ray diffractogram is different from the (111) orientation typically reported for Cu_2O films grown on non-matched substrates. Yet, it has already been obtained for Cu_2O films grown by MOCVD using also $Cu(hfac)_2$ as precursor.[27] This texture suggests the possibility of a local epitaxy between the Cu_2O and ZnO films. In order to verify the latter, high resolution transmission electron micrographs (HR-TEM) were taken at the interface between Cu_2O and ZnO. The continuity of the lattice planes in the TEM micrograph (Figure 5a) and of the FFT patterns taken across the Cu_2O/ZnO interface (Figure 5b - d) prove a local epitaxial relationship with [110] Cu_2O || [001] ZnO out-of-plane, and [001] Cu_2O || [010] ZnO in-plane orientation.

A schematic model of this epitaxial relationship is shown in Figure 5 e, f. The oxygen atoms at (001) planes of ZnO and the Cu atoms at (110) planes of Cu_2O form rectangular unit cells with sides ($\sqrt{3}\ a_{ZnO}$, $a_{ZnO} = 3.250$ Å) and ($\sqrt{2}\ a_{Cu_2O}$, $a_{Cu_2O} = 4.269$ Å), respectively, as represented with dashed lines in Figure 5 e. Under this configuration, the lattice mismatch f_o^1 corresponding to the [$\bar{1}$10] Cu_2O direction, that is, between the ($\bar{1}$10) Cu_2O and (100) ZnO planes is 7.3 % and the f_o^2 corresponding to the [001] Cu_2O direction, i.e. between (001) Cu_2O and (1$\bar{2}$0) ZnO planes, is as high as 31%. Nevertheless, epitaxy is still possible in a system with such a large lattice misfit thanks to domain matching epitaxy (DME), that occurs when integer multiples of lattice planes match at the interface of the films.[28] In fact, since $a_{Cu_2O}/a_{ZnO} = 1.31 \approx (n+1)/n$ with $n = 3$, coincidence occurs every 3 rectangular unit cells of Cu_2O and 4 of ZnO, as schematically depicted in Figure 5 g (black arrows indicate the coincidence sites). Looking at the coincidence lattice, the

f_o^2 natural misfit of 31 % is significantly reduced to $f_o^2 = (3a_{Cu_2O} - 4a_{ZnO})/4a_{ZnO} = 1.46\%$. As can be seen from Figure 5 g there is an extra ZnO plane for each unit cell of the coincidence lattice. The formation of a geometrical misfit dislocation at the interface relieves the lattice misfit strain, allowing lattice fitting and hetero-epitaxial growth. [27,29]

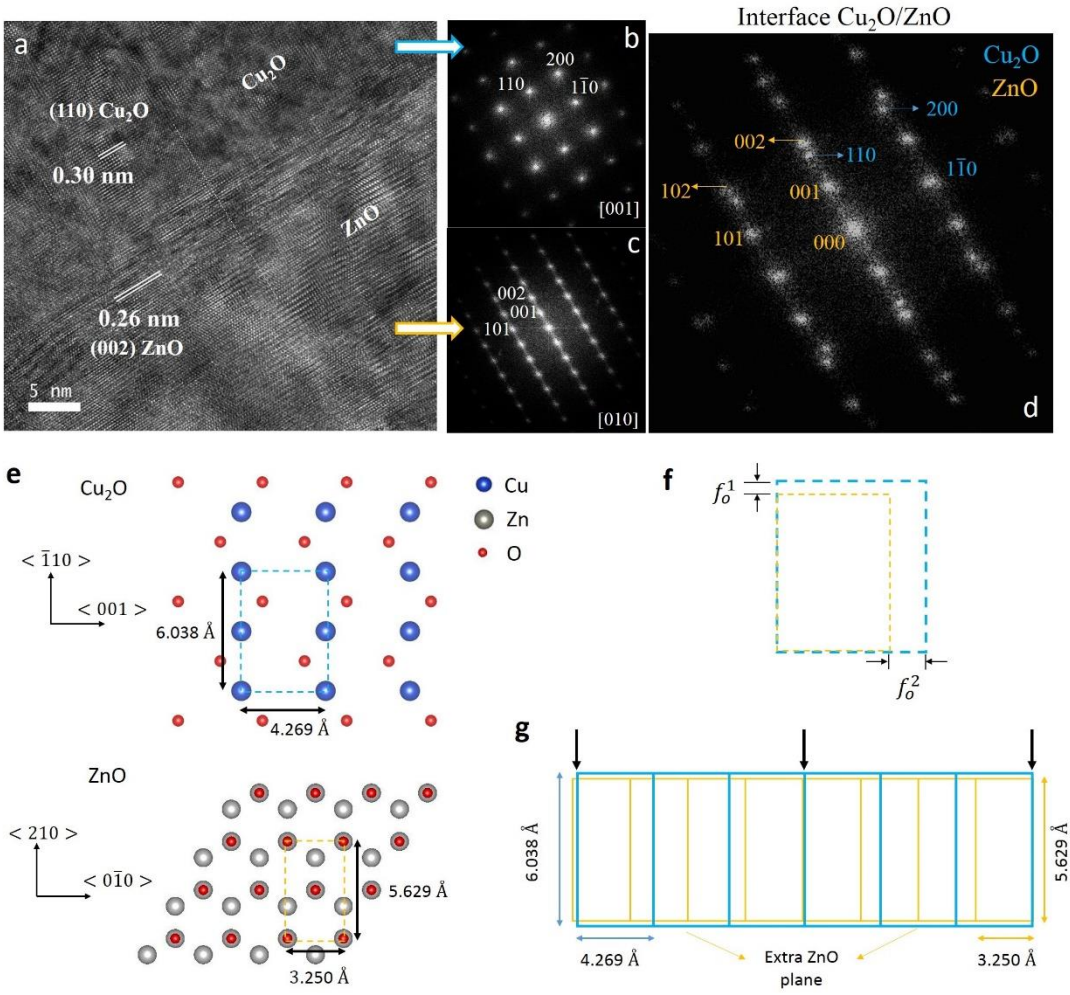

Figure 5. (a) HR-TEM micrograph taken at the Cu_2O/ZnO interface. (b, c, d) FFT patterns of the TEM image in the region of Cu_2O (b), ZnO (c), and at the interface (d). (e) Schematic model for the atomic arrangement of the (110) planes of Cu_2O (top) and the (001) planes of ZnO (bottom). (f) Top view schematic of the rectangular unit cells for Cu_2O and ZnO, indicating the lattice

mismatch. (g) Schematic model of the epitaxial relationship between the (110) Cu_2O and the (001) ZnO surfaces.

This local epitaxial relationship allows the growth of a high quality Cu_2O layer, which results in higher mobility and higher carrier's diffusion length due to lower defect density in the Cu_2O layer and at the heterojunction interface.

Optical and electrical properties of Cu_2O and ZnO the films

The optical and electrical properties of the n-type ZnO and p-type Cu_2O are essential for the junction performance through light absorption, electron-hole pair generation, and charge transport processes.

Ellipsometric measurements were performed to the samples in the 0.6 eV - 4.5 eV spectral range. A schematic of the physical model employed is shown in Figure 6b. The model consists of a three-layer structure on top of a Si substrate. For the Cu_2O layer, it was necessary to consider an uppermost layer composed of 50% Cu_2O and 50% voids in order to take into account the roughness at the surface.

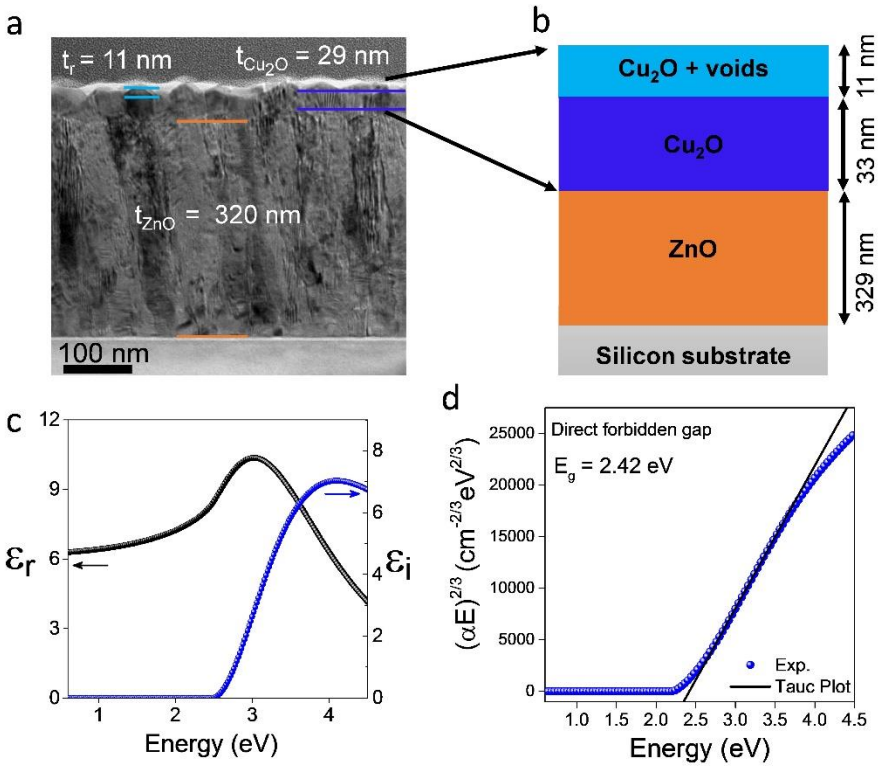

Figure 6. (a) TEM micrograph of the Cu_2O/ZnO lamella. (b) Schema of the physical model used for fitting the ellipsometric measurements. (c, d) Real and imaginary part of the dielectric function of the Cu_2O layer determined by ellipsometry (c) and Tauc Plot (d).

The values obtained for the thickness of the Cu_2O and ZnO layers are shown in Figure 6b. These values are in good agreement with those measured directly form the cross-section TEM micrograph presented in Figure 6a. Real (ε_r) and imaginary (ε_i) parts of the dielectric function, extracted from the fitting of ellipsometry measurements are shown in Figure 6c (see Supporting Information for more details). The band gap of the Cu_2O film was determined from the Tauc Plot (see Figure 6d). Cu_2O is a semiconductor with a direct forbidden band gap,[30] direct transition from the highest valence band maxima to the lowest conduction band minima is parity forbidden.[31] Therefore, an exponent of 2/3 was used for the Tauc plot in this case. Values around 2.42 eV were

obtained for the Cu_2O films in good agreement with the values reported in the literature for this material.[30]

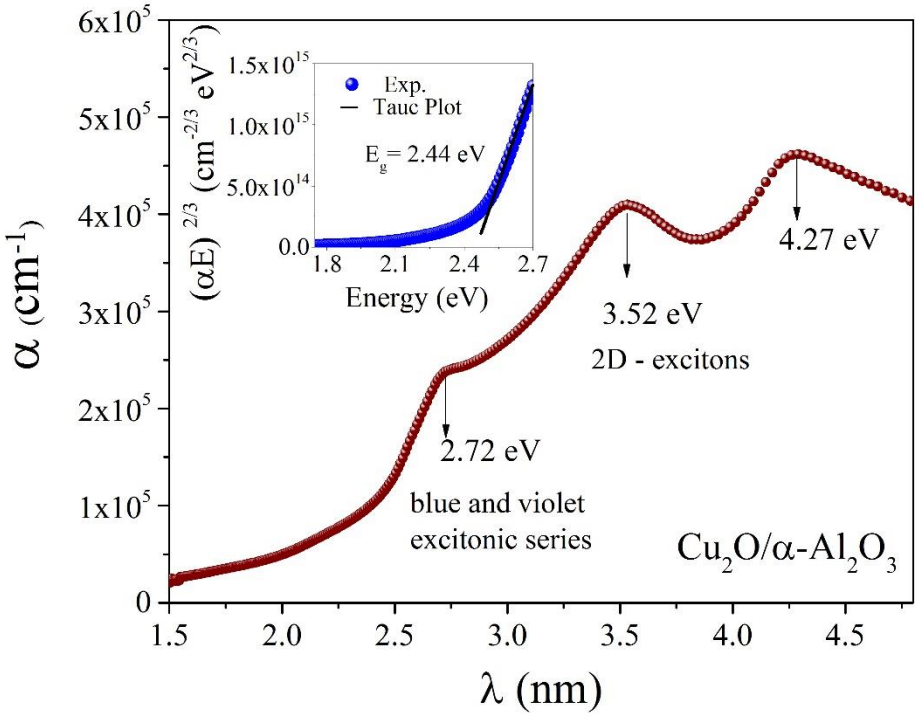

Figure 7. Absorption coefficient for the Cu_2O film deposited on sapphire and Tauc Plot as inset.

Transmittance and reflectance measurements were also performed to Cu_2O films deposited on α-Al_2O_3. In Figure 7 is shown the absorption coefficient of the films. The change in slope observed at 2.35 eV in the absorption spectrum is due of the contribution of the blue and violet excitonic series to the absorption of Cu_2O.[32] The contribution at 2.72 eV corresponds very well to the violet excitonic series.[31] Finally, the peaks located around 3.52 and 4.27 are associated to the 2D excitonic transitions.[33] The possibility to observe the excitonic peaks at room temperature is due to the high exciton binding energy for Cu_2O (~150 meV) and the good crystalline quality of the Cu_2O films deposited by ALD. The band gap value obtained from this sample is 2.44 eV, in good agreement with the values obtained by ellipsometry (see Figure 7 inset).

The band gap of the ZnO film was also determined from transmittance measurements, and a value of 3.16 eV was obtained from the Tauc Plot considering in this case a direct transition (see Figure S2 of Supporting information). This value is smaller compared with the typical values of ca. 3.37 eV reported for ZnO. However, a red shift of the optical bang gap of ZnO films deposited by reactive magnetron sputtering has been reported when decreasing the oxygen partial pressure, related with the oxygen vacancies content in the film.[34]

Four point probes measurements were performed in order to determine the resistivity of the Cu_2O films. The typical values reported in the literature for this material change widely depending on growth conditions and range from 10 to 10^5 Ω cm.[35,36] Values between 7-61 Ω cm have also been reported for sputtered Cu_2O samples after air-annealing between 200 and 300 °C (thicknesses ~ 820 nm)[30] and values around 125 Ω cm have been obtained for Cu_2O thin films (~100 nm) deposited by atmospheric ALD.[37] In our case, the resistivity values were in the range 9 – 150 Ω cm (Cu_2O films thickness of 40 - 60 nm), in good agreement with the best ones described previously. Hall effect measurements were performed to the Cu_2O film of lowest resistivity and the values of carriers concentration and mobility are $4 \times 10^{16}\, cm^{-3}$ and $19\ cm^2/Vs$, respectively. This low resistivity and high mobility values are explained by the high crystalline quality of the Cu_2O film reported above. Furthermore, the large size of Cu_2O grains (~100-200 nm) observed in the top-view SEM micrograph also contributes to high mobility, since electron scattering at grain boundaries is reduced.[37–39]

For the ZnO films, resistivity values change widely with the oxygen partial pressure and the position of the substrate in the substrate holder.[25] In particular, the ZnO films used for the fabrication of the heterojunction showed resistivity values of 90 Ω cm. The Hall measurements performed to this sample were very unstable and for this reason are not reported here.

Optical and electrical characterization of the heterojunctions

For the optical and electrical characterization of the junctions, a Cu_2O (40 nm) / ZnO (250 nm) heterojunction was deposited on top of an ITO/glass substrate. The transmittance spectrum of the Cu_2O/ZnO heterojunction is displayed in Figure 8a. The black line corresponds to the sputtered ZnO thin film alone and the blue line is after the deposition of Cu_2O by ALD. Oscillations are due to optical interference phenomenon. The average transmittance (AVT) of the system was determined following the same approach that is employed in window technology and is described by the following equation [15]:

$$AVT = \frac{\int T(\lambda)P(\lambda)S(\lambda)d\lambda}{\int P(\lambda)S(\lambda)\,d\lambda}$$

Where λ is the wavelengh, T the transmittance of the sample, P is the photopic response of the human eye (Figure 8 a, violet line), and S the Solar flux (AM1.5G). An AVT of 73 % was obtained when integrating over the visible range of the electromagnetic spectrum (400 - 700 nm).[40] A picture of the sample is shown at the inset of Figure 8a. The left side (yellow-brown) corresponds to the Cu_2O/ZnO junction and the right side is the uncovered ZnO film (this region was masked during ALD deposition). To verify the rectifying behavior of the Cu_2O/ZnO heterojunction, electrical measurements were performed to the samples. The contacts to the sample were done through two metallic needles as is also displayed in the schematic of Figure 8 b, inset. Figure 8 b shows the current density – voltage (J-V) characteristics of the sample. A non-linear rectifying behavior is observed, demonstrating the formation of a p-n junction between the Cu_2O and the ZnO. A turn-on voltage of 1.1 V is measured form the J-V curve, consistent with the value measured for Cu_2O-ZnO nanojunctions reported in our previous work.[25]

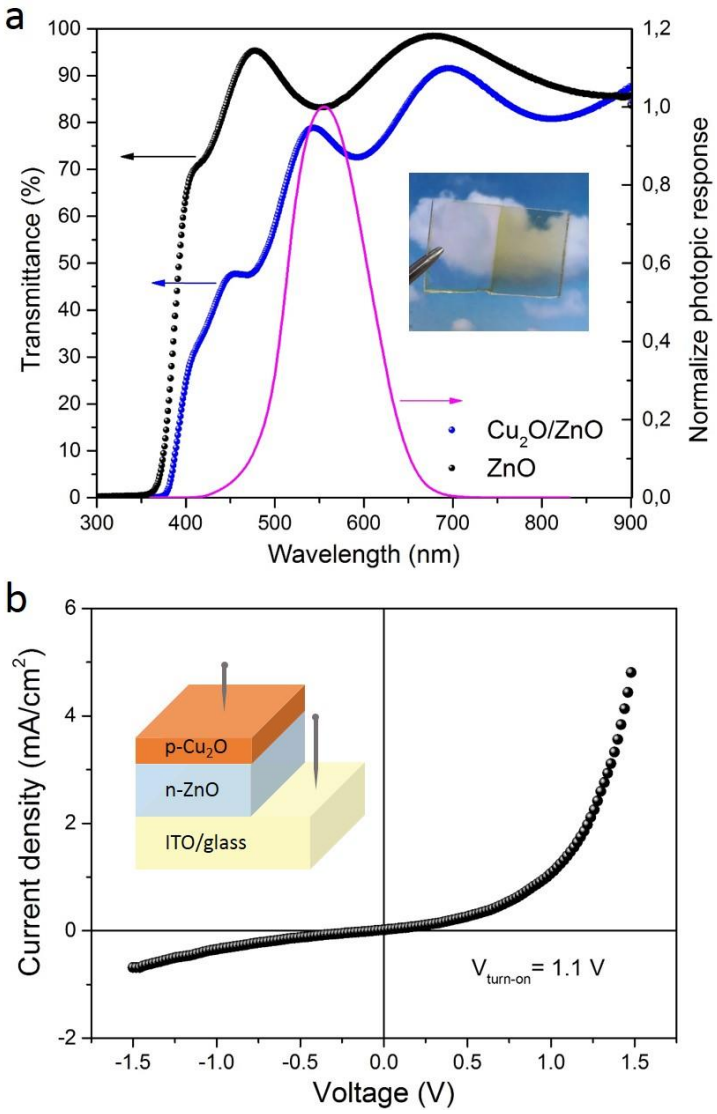

Figure 8. (a) Transmittance of the ZnO film (black), Cu_2O/ZnO film (blue) and the normalize photopic response of the human eye (magenta), the inset is a picture of the sample to illustrate the transparency, the left side corresponds to the Cu_2O/ZnO junction and the right side to the ZnO film alone. (b) Current density-voltage characteristics of the p-Cu_2O/n-ZnO/ITO junction, schematic of the sample configuration for the measurement at the inset.

In order to analyze the photo-response of the heterojunction, J-V characteristics were measured by exposing the sample to 1 Sun illumination. As can be seen in Figure 9 a, there is an enhancement

of the current under both forward and reverse voltages. Short circuit current density ($J_{sc} = 34.7\ \mu A/cm^2$) and open circuit voltage ($V_{OC} = 72\ mV$) where measured from the magnified J-V curved at the inset of Figure 9 a.

Table 1. Figures of merit of ZnO-based photodetectors.

Heterojunction	Photocurrent	Responsivity	Response time	Recovery time	V	Detection Range	Ref.
Cu_2O/ZnO Core-shell nanowires	0.80 μA/cm^2	7.67 μA/W	< 0.09 s	< 0.09 s	0 V	VIS	[5]
Cu_2O/ZnO nanorods	~ 6 μA	~ 70 mA/W	0.075 s	0.070 s	0 V	UV-Blue	[23]
Cu_2O/ZnO nanorods	~15 μA	-	0.22 s	0.32 s	0 V	VIS	[41]
CdS/AZO nanorods/polymer	23.29 mA/cm^2	50 A/W	22 s	17 s	5 V	VIS	[42]
NiO/ZnO films	~ 50 pA	0.415 mA/W	7.5 s	4.8 s	0 V	UV	[21]
NiO/ZnO films	~ 10 mA/cm^2	10.2 A/W	0.2 s	0.18 s	-1 V	UV	[43]
ZnO/TiO_2 Core-shell	360 μA/ cm^2	0.4 A/W	0.022 s	0.009 s	0 V	UV	[22]
ZnO nanowires/SnS	144 nA	364 μA/W	0.4 s	0.2 s	0 V	VIS	[19]
Nanoscale Cu_2O/ZnO films	34.7 μA/ cm^2 (at 0 V) 3.9 mA/cm^2 (at 1.5 V)	0.28 mA/W (at 0 V) 39 mA/W (at 1.5 V)	0.15 s	0.15 s	0 V	VIS	This work

Responsivity was calculated by, $R = \frac{J_{ph}}{P_{opt}}$, where P_{opt} is the incident optical power density on the device, and $J_{ph} = J_{light} - J_{dark}$, is the photo-generated current density in the device. A maximum responsivity of $39\ mA/W$ is obtained at a forward bias voltage of 1.5 V. Additionally, the heterojunction shows a stable self-powered photoresponse at 0 bias voltage, as can be seen in Figure 9 a, b. The responsivity at 0 bias voltage was of $0.28\ mA/W$. Higher responsivities have been achieved from other ZnO-based devices reported in Table 1. However, we need to take into

account the fact that we fabricated a semi-transparent heterojunction, therefore a compromise need to be achieved between electrical performance and transparency. The response time of the system was calculated as the time required to transit from 10% to 90% of maximum amplitude of the current pulse (Figure 9 b, inset). Values around 0.10 to 0.15 s were measured from several pulses, which are faster than other oxide-based visible photodetectors (see Table 1), and are in relatively good agreement with the values obtained for some nanostructured Cu_2O/ZnO photodetectors.

A schematic of the band energy diagram for the isolated Cu_2O and ZnO semiconductors is depicted in Figure 9 c. The values of electron affinity were taken from the literature,[44] and the bandgaps are those determined from ellipsometry and UV-VIS spectroscopy. A schematic of the energy band bending at the heterojunction interface is depicted in Figure 9 d, illustrating the mechanism of photocurrent generation at zero bias voltage. Electron-hole pairs generated after light absorption in Cu_2O are separated at the space-charge region by the built-in electric field and collected at the electrodes, producing the photocurrent observed in Figure 9 b.

In summary, the local epitaxial growth of Cu_2O on ZnO, together with the high quality, low resistivity, and high hole mobility of the Cu_2O films obtained here are promising for all-oxide optoelectronic applications. Even if ALD is a slow process not suitable for growing thick Cu_2O films, it can serve as high quality buffer layer. Furthermore, it has the advantages of large scale scalability and possible incorporation into nanostructured devices where conformability is a fundamental factor and no thick layers of Cu_2O are needed.

The stable and fast self-powered photoresponse makes the Cu_2O/ZnO heterojunctions reported here highly suitable for photodetection. The self-powered photoresponse allows the detection of the incoming light and at the same time is exploited to power the device, without the need of an external power supply, thanks to the photovoltaic effect at the p-n junction. This makes the device

self-sustainable, allows to reduce its cost, enhances it adaptability, and reduces energy consumption, which is highly sought nowadays in many fields in which photodetectors are employed, e.g. fiber-optics communications, optical receivers, and environmental sensors, and will be indispensable in the future for "smart" sensor technology and photodetector networks.

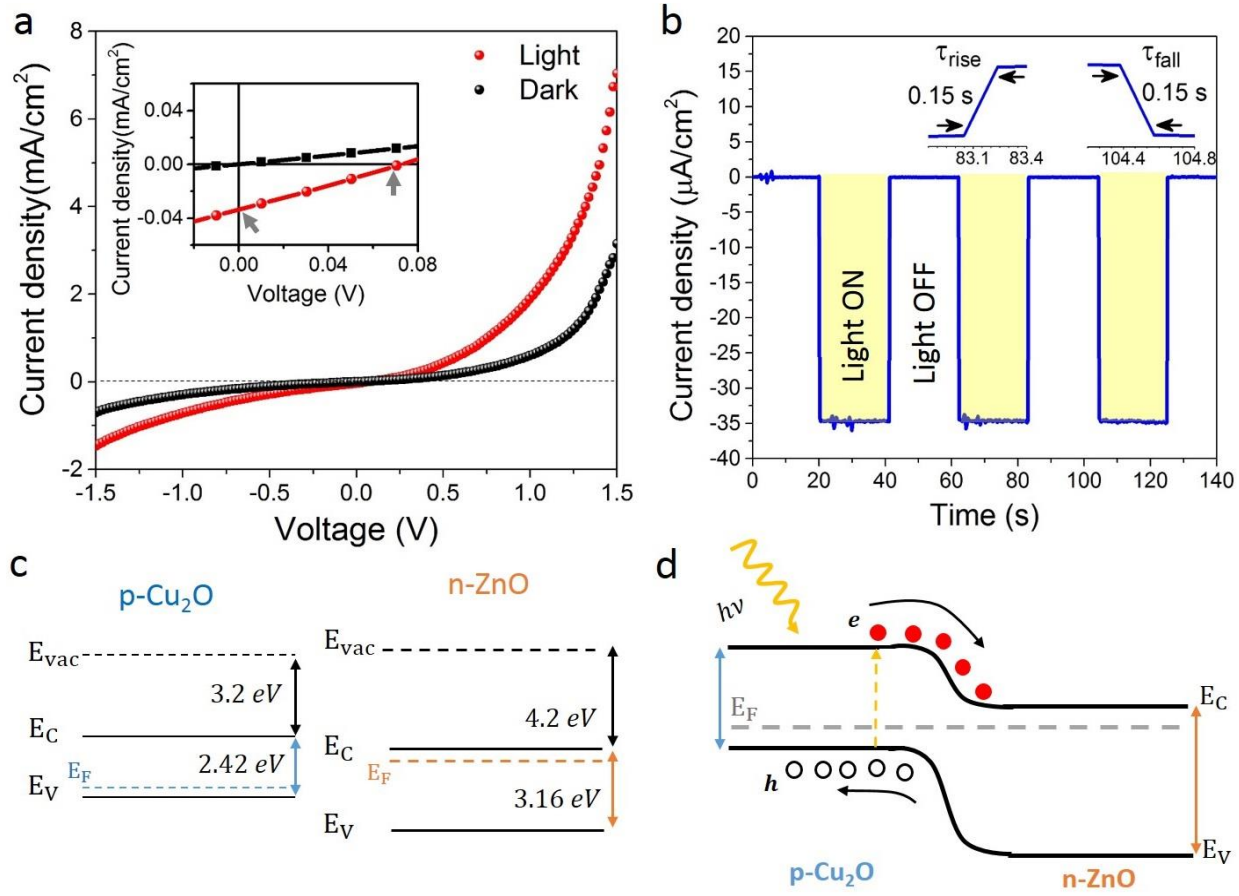

Figure 9. (a) Current density - voltage (J-V) characteristics of the Cu_2O/ZnO heterojunction in dark and under 1 Sun illumination with a magnified J-V curve as inset where the open circuit voltage and short circuit current are indicated (gray arrows). (b) Current density vs. time at 0 bias voltage, during multiples dark/light cycles of approximately 20 s, the response time is indicated at the inset. (c) Energy band diagram of the Cu_2O and ZnO isolated semiconductors. (d) Schematic of the band bending for the Cu_2O/ZnO heterojunction and the mechanism for the photocurrent generation under 1 Sun illumination at 0 bias voltage.

Conclusion

In this work, we reported on the fabrication of transparent thin film p-Cu_2O/n-ZnO nanoscale-heterojunctions. The morphology and structure of the films was studied by SEM, DRX and TEM, showing a high crystalline quality, and local epitaxial relation between both materials. The optical responses and the bandgap of the films were determined by ellipsometry and transmittance measurements, giving a value of 2.42 eV for Cu_2O and 3.16 eV for ZnO. Electrical characterization of the Cu_2O films show relatively high carrier concentration of ~ 10^{16} cm^{-3}, very low resistivity of 9 - 150 Ω cm, and high mobility values of 19 cm^2/ Vs. Transmittance measurements performed to the heterojunction show high transparency in the visible range, holding promises for all-oxides transparent electronics. Furthermore, the heterojunctions show a photoconductive behavior, and a stable and fast self-powered photoresponse, under 1 Sun illumination, highly sought for visible photodetection.

ASSOCIATED CONTENT

Supporting Information. Ellipsometric models and fitting, Tauc Plot of the ZnO film, contact area estimation (PDF).

AUTHOR INFORMATION

Corresponding Author

David Horwat

*E-mail: david.horwat@univ-lorraine.fr

Author Contributions

The manuscript was written through contributions of all authors. DH, MJ, FMu, FMo, JFP planned and supervised the study. SM prepared the FIB lamella and JG performed the TEM measurements. FR, NA and AV performed the macroscopic electrical measurements to the heterojunctions. YB and AE performed the ellipsometric measurements and modeling. CDM conducted the experiments and wrote the manuscript. All authors have given approval to the final version of the manuscript

Funding Sources

Erasmus Mundus Ph.D. fellowship doctoral program DocMASE (Project 2015-03)

Université franco-allemande (UFA) PhD track "German/French Graduate School in Materials Science and Engineering" (PhD02-14)

Carl Tryggers Foundation (CTS16:13, CTS17:24)

Kempe Foundations (SMK-2546)

Knut and Alice Wallenberg Foundation

Notes

The authors declare no competing financial interest.

ACKNOWLEDGMENT

The Davm competence center at Institut Jean Lamour is acknowledged for allowing the access to the ALD deposition facility. C. de Melo would like to thank the European Commission for the “Erasmus Mundus” Ph.D. fellowship within the DocMASE doctoral program and to the UFA

(*Université franco-allemande*) for the mobility aids and the *cotutelle* financial aids. F. Rigoni thanks the Carl Tryggers Foundation for the postdoctoral fellowship.

ABBREVIATIONS

ALD, atomic layer deposition; TCO, transparent conductive oxide; GPC, growth per cycle; SEM, scanning electron microscopy; FIB, focused ion beam; TEM, transmission electron microscopy; EDS, energy dispersive spectroscopy; HR-TEM, high resolution transmission electron microscopy; FFT, fast Fourier transform pattern; DME, domain matching epitaxy; AVT, average transmittance.

REFERENCES

(1) Janotti, A.; Van de Walle, C. G. Fundamentals of Zinc Oxide as a Semiconductor. *Rep. Prog. Phys.* **2009**, *72* (12), 126501. https://doi.org/10.1088/0034-4885/72/12/126501.

(2) Minami, T.; Nishi, Y.; Miyata, T.; Nomoto, J. High-Efficiency Oxide Solar Cells with ZnO/Cu_2O Heterojunction Fabricated on Thermally Oxidized Cu_2O Sheets. *Appl. Phys. Express* **2011**, *4* (6), 062301. https://doi.org/10.1143/APEX.4.062301.

(3) Rühle, S.; Anderson, A. Y.; Barad, H.-N.; Kupfer, B.; Bouhadana, Y.; Rosh-Hodesh, E.; Zaban, A. All-Oxide Photovoltaics. *J. Phys. Chem. Lett.* **2012**, *3* (24), 3755–3764. https://doi.org/10.1021/jz3017039.

(4) Zhang, Z.; Wang, P. Highly Stable Copper Oxide Composite as an Effective Photocathode for Water Splitting via a Facile Electrochemical Synthesis Strategy. *J. Mater. Chem.* **2012**, *22* (6), 2456–2464. https://doi.org/10.1039/C1JM14478B.

(5) Ghamgosar, P.; Rigoni, F.; You, S.; Dobryden, I.; Kohan, M. G.; Pellegrino, A. L.; Concina, I.; Almqvist, N.; Malandrino, G.; Vomiero, A. ZnO-Cu_2O Core-Shell Nanowires as

Stable and Fast Response Photodetectors. *Nano Energy* **2018**, *51*, 308–316. https://doi.org/10.1016/j.nanoen.2018.06.058.

(6) Ouyang, W.; Teng, F.; He, J.-H.; Fang, X. Enhancing the Photoelectric Performance of Photodetectors Based on Metal Oxide Semiconductors by Charge-Carrier Engineering. *Adv. Funct. Mater.* **2019**, *29* (9), 1807672. https://doi.org/10.1002/adfm.201807672.

(7) Galstyan, V.; Ponzoni, A.; Kholmanov, I.; Natile, M. M.; Comini, E.; Nematov, S.; Sberveglieri, G. Reduced Graphene Oxide–TiO_2 Nanotube Composite: Comprehensive Study for Gas-Sensing Applications. *ACS Appl. Nano Mater.* **2018**, *1* (12), 7098–7105. https://doi.org/10.1021/acsanm.8b01924.

(8) Rovisco, A.; Branquinho, R.; Martins, J.; Oliveira, M. J.; Nunes, D.; Fortunato, E.; Martins, R.; Barquinha, P. Seed-Layer Free Zinc Tin Oxide Tailored Nanostructures for Nanoelectronic Applications: Effect of Chemical Parameters. *ACS Appl. Nano Mater.* **2018**, *1* (8), 3986–3997. https://doi.org/10.1021/acsanm.8b00743.

(9) Zhang, K.; Wang, Z. L.; Yang, Y. Enhanced P3HT/ZnO Nanowire Array Solar Cells by Pyro-Phototronic Effect. *ACS Nano* **2016**, *10* (11), 10331–10338. https://doi.org/10.1021/acsnano.6b06049.

(10) Ievskaya, Y.; Hoye, R. L. Z.; Sadhanala, A.; Musselman, K. P.; MacManus-Driscoll, J. L. Fabrication of ZnO/Cu_2O Heterojunctions in Atmospheric Conditions: Improved Interface Quality and Solar Cell Performance. *Sol. Energy Mater. Sol. Cells* **2015**, *135*, 43–48. https://doi.org/10.1016/j.solmat.2014.09.018.

(11) Pavan, M.; Rühle, S.; Ginsburg, A.; Keller, D. A.; Barad, H.-N.; Sberna, P. M.; Nunes, D.; Martins, R.; Anderson, A. Y.; Zaban, A.; et al. TiO_2/Cu_2O All-Oxide Heterojunction Solar Cells

Produced by Spray Pyrolysis. *Sol. Energy Mater. Sol. Cells* **2015**, *132*, 549–556. https://doi.org/10.1016/j.solmat.2014.10.005.

(12) Minami, T.; Nishi, Y.; Miyata, T. Heterojunction Solar Cell with 6% Efficiency Based on an N-Type Aluminum–gallium–oxide Thin Film and p-Type Sodium-Doped Cu_2O Sheet. *Appl. Phys. Express* **2015**, *8* (2), 022301. https://doi.org/10.7567/APEX.8.022301.

(13) Zuo, C.; Ding, L. Solution-Processed Cu_2O and CuO as Hole Transport Materials for Efficient Perovskite Solar Cells. *Small* **2015**, *11* (41), 5528–5532. https://doi.org/10.1002/smll.201501330.

(14) Nordseth, Ø.; Kumar, R.; Bergum, K.; Fara, L.; Foss, S. E.; Haug, H.; Drăgan, F.; Crăciunescu, D.; Sterian, P.; Chilibon, I.; et al. Optical Analysis of a ZnO/Cu_2O Subcell in a Silicon-Based Tandem Heterojunction Solar Cell. *Green Sustain. Chem.* **2017**, *07*, 57. https://doi.org/10.4236/gsc.2017.71005.

(15) Traverse, C. J.; Pandey, R.; Barr, M. C.; Lunt, R. R. Emergence of Highly Transparent Photovoltaics for Distributed Applications. *Nat. Energy* **2017**, *2* (11), 849–860. https://doi.org/10.1038/s41560-017-0016-9.

(16) Deo, M.; Mujawar, S.; Game, O.; Yengantiwar, A.; Banpurkar, A.; Kulkarni, S.; Jog, J.; Ogale, S. Strong Photo-Response in a Flip-Chip Nanowire p-Cu_2O/n-ZnO Junction. *Nanoscale* **2011**, *3* (11), 4706–4712. https://doi.org/10.1039/C1NR10665A.

(17) Bai, Z.; Zhang, Y. Self-Powered UV–visible Photodetectors Based on ZnO/Cu_2O Nanowire/Electrolyte Heterojunctions. *J. Alloys Compd.* **2016**, *675*, 325–330. https://doi.org/10.1016/j.jallcom.2016.03.051.

(18) Wang, Z. L. Self-Powered Nanosensors and Nanosystems. *Adv. Mater.* **2012**, *24* (2), 280–285. https://doi.org/10.1002/adma.201102958.

(19) Ouyang, B.; Zhang, K.; Yang, Y. Photocurrent Polarity Controlled by Light Wavelength in Self-Powered ZnO Nanowires/SnS Photodetector System. *iScience* **2018**, *1*, 16–23. https://doi.org/10.1016/j.isci.2018.01.002.

(20) Tian, W.; Wang, Y.; Chen, L.; Li, L. Self-Powered Nanoscale Photodetectors. *Small* **2017**, *13* (45), 1701848. https://doi.org/10.1002/smll.201701848.

(21) Zhang, Z.; Ning, Y.; Fang, X. From Nanofibers to Ordered ZnO/NiO Heterojunction Arrays for Self-Powered and Transparent UV Photodetectors. *J. Mater. Chem. C* **2019**, *7* (2), 223–229. https://doi.org/10.1039/C8TC05877F.

(22) Gao, C.; Li, X.; Wang, Y.; Chen, L.; Pan, X.; Zhang, Z.; Xie, E. Titanium Dioxide Coated Zinc Oxide Nanostrawberry Aggregates for Dye-Sensitized Solar Cell and Self-Powered UV-Photodetector. *J. Power Sources* **2013**, *239*, 458–465. https://doi.org/10.1016/j.jpowsour.2013.04.003.

(23) Wang, C.; Xu, J.; Shi, S.; Zhang, Y.; Gao, Y.; Liu, Z.; Zhang, X.; Li, L. Optimizing Performance of Cu_2O/ZnO Nanorods Heterojunction Based Self-Powered Photodetector with ZnO Seed Layer. *J. Phys. Chem. Solids* **2017**, *103*, 218–223. https://doi.org/10.1016/j.jpcs.2016.12.026.

(24) Bai, Z.; Liu, J.; Liu, F.; Zhang, Y. Enhanced Photoresponse Performance of Self-Powered UV–visible Photodetectors Based on ZnO/Cu_2O/Electrolyte Heterojunctions via Graphene Incorporation. *J. Alloys Compd.* **2017**, *726*, 803–809. https://doi.org/10.1016/j.jallcom.2017.08.035.

(25) de Melo, C.; Jullien, M.; Ghanbaja, J.; Montaigne, F.; Pierson, J.-F.; Soldera, F.; Rigoni, F.; Almqvist, N.; Vomiero, A.; Mücklich, F.; et al. Local Structure and Point-Defect-Dependent Area-Selective Atomic Layer Deposition Approach for Facile Synthesis of p-Cu_2O/n-ZnO

Segmented Nanojunctions. *ACS Appl. Mater. Interfaces* **2018**, *10* (43), 37671–37678. https://doi.org/10.1021/acsami.8b12584.

(26) de Melo, C.; Jullien, M.; Battie, Y.; En Naciri, A.; Ghanbaja, J.; Montaigne, F.; Pierson, J.-F.; Rigoni, F.; Almqvist, N.; Vomiero, A.; et al. Tunable Localized Surface Plasmon Resonance and Broadband Visible Photoresponse of Cu Nanoparticles/ZnO Surfaces. *ACS Appl. Mater. Interfaces* **2018**, *10* (47), 40958–40965. https://doi.org/10.1021/acsami.8b17194.

(27) Jeong, S.; Aydil, E. S. Heteroepitaxial Growth of Cu_2O Thin Film on ZnO by Metal Organic Chemical Vapor Deposition. *J. Cryst. Growth* **2009**, *311* (17), 4188–4192. https://doi.org/10.1016/j.jcrysgro.2009.07.020.

(28) Narayan, J.; Larson, B. C. Domain Epitaxy: A Unified Paradigm for Thin Film Growth. *J. Appl. Phys.* **2002**, *93* (1), 278. https://doi.org/10.1063/1.1528301.

(29) Trampert, A.; Ploog, K. h. Heteroepitaxy of Large-Misfit Systems: Role of Coincidence Lattice. *Cryst. Res. Technol.* **2000**, *35* (6–7), 793–806. https://doi.org/10.1002/1521-4079(200007)35:6/7<793::AID-CRAT793>3.0.CO;2-3.

(30) Wang, Y.; Miska, P.; Pilloud, D.; Horwat, D.; Mücklich, F.; Pierson, J. F. Transmittance Enhancement and Optical Band Gap Widening of Cu_2O Thin Films after Air Annealing. *J. Appl. Phys.* **2014**, *115* (7), 073505. https://doi.org/10.1063/1.4865957.

(31) Meyer, B. K.; Polity, A.; Reppin, D.; Becker, M.; Hering, P.; Klar, P. J.; Sander, T.; Reindl, C.; Benz, J.; Eickhoff, M.; et al. Binary Copper Oxide Semiconductors: From Materials towards Devices. *Phys. Status Solidi B* **2012**, *249* (8), 1487–1509. https://doi.org/10.1002/pssb.201248128.

(32) Malerba, C.; Biccari, F.; Leonor Azanza Ricardo, C.; D'Incau, M.; Scardi, P.; Mittiga, A. Absorption Coefficient of Bulk and Thin Film Cu_2O. *Sol. Energy Mater. Sol. Cells* **2011**, *95* (10), 2848–2854. https://doi.org/10.1016/j.solmat.2011.05.047.

(33) Ito, T.; Kawashima, T.; Yamaguchi, H.; Masumi, T.; Adachi, S. Optical Properties of Cu_2O Studied by Spectroscopic Ellipsometry. *J. Phys. Soc. Jpn.* **1998**, *67* (6), 2125–2131. https://doi.org/10.1143/JPSJ.67.2125.

(34) Liu, H.; Zeng, F.; Lin, Y.; Wang, G.; Pan, F. Correlation of Oxygen Vacancy Variations to Band Gap Changes in Epitaxial ZnO Thin Films. *Appl. Phys. Lett.* **2013**, *102* (18), 181908. https://doi.org/10.1063/1.4804613.

(35) De Los Santos Valladares, L.; Salinas, D. H.; Dominguez, A. B.; Najarro, D. A.; Khondaker, S. I.; Mitrelias, T.; Barnes, C. H. W.; Aguiar, J. A.; Majima, Y. Crystallization and Electrical Resistivity of Cu_2O and CuO Obtained by Thermal Oxidation of Cu Thin Films on SiO_2/Si Substrates. *Thin Solid Films* **2012**, *520* (20), 6368–6374. https://doi.org/10.1016/j.tsf.2012.06.043.

(36) Chu, C.-L.; Lu, H.-C.; Lo, C.-Y.; Lai, C.-Y.; Wang, Y.-H. Physical Properties of Copper Oxide Thin Films Prepared by Dc Reactive Magnetron Sputtering under Different Oxygen Partial Pressures. *Phys. B Condens. Matter* **2009**, *404* (23), 4831–4834. https://doi.org/10.1016/j.physb.2009.08.185.

(37) Muñoz-Rojas, D.; Jordan, M.; Yeoh, C.; Marin, A. T.; Kursumovic, A.; Dunlop, L. A.; Iza, D. C.; Chen, A.; Wang, H.; MacManus Driscoll, J. L. Growth of ~ 5 $Cm^2 V^{-1} s^{-1}$ Mobility, p-Type Copper(I) Oxide (Cu_2O) Films by Fast Atmospheric Atomic Layer Deposition (AALD) at 225°C and Below. *AIP Adv.* **2012**, *2* (4), 042179. https://doi.org/10.1063/1.4771681.

(38) Horwat, D.; Billard, A. Effects of Substrate Position and Oxygen Gas Flow Rate on the Properties of ZnO: Al Films Prepared by Reactive Co-Sputtering. *Thin Solid Films* **2007**, *515* (13), 5444–5448. https://doi.org/10.1016/j.tsf.2006.12.188.

(39) Gall, D. Electron Mean Free Path in Elemental Metals. *J. Appl. Phys.* **2016**, *119* (8), 085101.

(40) Gunter Wyszecki; W. S. Stiles. *Color Science: Concepts and Methods, Quantitative Data and Formulae*, 2nd ed.; John Wiley and Sons: New York, 1982.

(41) Lin, P.; Chen, X.; Yan, X.; Zhang, Z.; Yuan, H.; Li, P.; Zhao, Y.; Zhang, Y. Enhanced Photoresponse of Cu_2O/ZnO Heterojunction with Piezo-Modulated Interface Engineering. *Nano Res.* **2014**, *7* (6), 860–868. https://doi.org/10.1007/s12274-014-0447-6.

(42) Dhar, S.; Chakraborty, P.; Majumder, T.; Mondal, S. P. CdS-Decorated Al-Doped ZnO Nanorod/Polymer Schottky Junction Ultraviolet–Visible Dual-Wavelength Photodetector. *ACS Appl. Nano Mater.* **2018**, *1* (7), 3339–3345. https://doi.org/10.1021/acsanm.8b00551.

(43) Kim, D. Y.; Ryu, J.; Manders, J.; Lee, J.; So, F. Air-Stable, Solution-Processed Oxide P–n Heterojunction Ultraviolet Photodetector. *ACS Appl. Mater. Interfaces* **2014**, *6* (3), 1370–1374. https://doi.org/10.1021/am4050019.

(44) Lahmar, H.; Azizi, A.; Schmerber, G.; Dinia, A. Effect of the Thickness of the ZnO Buffer Layer on the Properties of Electrodeposited P-Cu_2O/n-ZnO/n-AZO Heterojunctions. *RSC Adv.* **2016**, *6* (73), 68663–68674. https://doi.org/10.1039/C6RA04834J.